

To Study The Role Of Sigma Factor SigE In The Stringent Response Of *Mycobacterium Tuberculosis*

Babasaheb Shivanath Ghodke, Sakshi Yadav

Department of Microbiology, Dr. A.P.J. Abdul Kalam University, Indore, Madhya Pradesh, India.

Address For Correspondence: Babasaheb Shivanath Ghodke

Address: Department of Microbiology, Dr. A.P.J. Abdul Kalam University, Indore, Madhya Pradesh, India.

E-mail Address: bghodke1984@gmail.com

Abstract

Bacteria respond to nutrient deprivation by activating the stringent response, a stress signalling system that leads to metabolic remodelling and a reduction in growth rate and energy needs. The model of stringent response in *Mycobacterium tuberculosis* induced by growth in low phosphate is well-characterized. Prior research suggested that the extracytoplasmic function (ECF) sigma factor SigE plays a crucial role in the activation of the stringent response. Using RNA sequencing, we examine the temporal dynamics of the transcriptional response of a sigE mutant and its wild-type progenitor strain to low phosphate in this study. Both strains exhibited a typical stringent response to reduced phosphate, including the downregulation of genes encoding ribosomal proteins and RNA polymerase-ase. We also observed transcriptional alterations that support the occurrence of an energy imbalance, which was compensated by a decrease in the activity of the electron transport chain, a decrease in the export of protons, and a reorganisation of the central metabolism. The most notable difference between the two strains was the induction of multiple stress-related genes in the sigE mutant, specifically the genes encoding the ECF sigma factor SigH and the transcriptional regulator WhiB6. Since both proteins respond to redox imbalances, the induction of these proteins suggests that the sigE mutant is unable to maintain redox homeostasis in response to the energetics imbalance induced by low phosphate. In conclusion, our data imply that SigE is not directly involved in initiating stringent response, but rather in protecting the cell from stress resulting from exposure to low levels of phosphate and activation of stringent response.

Mycobacterium tuberculosis is capable of entering a quiescent state, which enables it to establish latent infections and develop resistance to antibacterial drugs. Due to the dearth of dependable animal models, the physiology of dormant bacteria and the mechanism(s) by which bacteria enter dormancy during an infection remain unknown. Nonetheless, several in vitro models that replicate the conditions encountered during an infection can reproduce distinct characteristics of dormancy (growth arrest, metabolic deceleration, and drug tolerance). The stringent response is one of them; it is a stress response programme that allows microbes to endure nutrient deprivation. In this study, we provide evidence that the sigma factor SigE is not directly involved in the activation of the stringent response, as was previously hypothesised. However, SigE is essential for assisting the bacteria in coping with the metabolic stress associated with the adaptation to low phosphate and activation of the stringent response.

Keywords: *Mycobacterium tuberculosis*, sigma factors, stringent response, transcriptional regulation

INTRODUCTION

Mycobacterium tuberculosis causes the infectious disease tuberculosis, which is spread through the air. In 2020, approximately 10 million new cases of tuberculosis will be reported, with 1,300,000 deaths.

Tuberculosis treatment necessitates the administration of numerous antimicrobials for months due to *M. tuberculosis*'s ability to remain in a latent state for extended periods of time, during which it develops drug tolerance and persistence. One of the primary mechanisms utilised by *M. tuberculosis* to develop drug tolerance is the stringent response, a complex reorganisation of metabolism designed to limit growth and energy requirements in order to survive for extended periods in starvation-like conditions. Alarmones (ppGpp), generated by Rel, a ribosome-associated protein, in response to specific signals such as the binding of a deacylated tRNA to ribosome site A, is the essential molecule for the development of stringent response. Among the most well-known models of stringent response in *M. tuberculosis* is the one induced by exposure to a low-phosphate environment (Fig. 1). Under these conditions, the two-component regulatory system SenX3-RegX3 activates the transcription of the phosphate-specific transport operon, *pstS3-pstC2-pstA1*, and of *ppk1*, a gene encoding a polyphosphate (polyP) kinase, resulting in an increase of polyP levels in the cell, a well-known stress signal. Accumulation of polyP facilitates the phosphorylation of MprB, the response regulator of the two-component system MprAB, which positively regulates the structural gene of the extracytoplasmic sigma factor SigE and is involved in the induction of *ppk* expression along with SenX3-RegX3. In these conditions, it has been proposed that SigE is also capable of regulating the expression of *relA*, thereby activating the stringent response. However, the majority of experiments that suggest *relA* transcription is directly dependent on SigE were conducted on *Mycobacterium smegmatis* and not on *M. tuberculosis*. Furthermore, it is known that the activation of the stringent response is predominantly regulated at the posttranslational level, rather than at the transcriptional level. These findings prompted us to investigate whether the true function of SigE induction under low phosphate conditions was to initiate the stringent response. To answer this question, we utilised RNA sequencing (RNA-seq) data to compare the transcriptional response dynamics to reduced phosphate of a sigE mutant and its wild-type parental strain. We found evidence that SigE is not directly involved in the development of the stringent response, as was previously hypothesised, because the main transcriptional signs of this response, such as the downregulation of genes encoding ribosomal proteins and RNA polymerase (RNAPol), were conserved between the two strains. Nevertheless, we discovered evidence that the function of SigE in these conditions is to protect the bacterium from the stress induced by the metabolic and structural alterations caused by the stringent response.

MATERIALS AND METHODS

Afin d'accroître la fiabilité et la reproductibilité de l'étude, les grandes recommandations en matière de conception d'RNA-seq experiments were implemented.

First, each strain of bacteria was cultured in triplicate at each time point. Particularly when dealing with time series data, replicates play a crucial role in the bioinformatics analyses that follow.

Before sequencing, ERCC spike-in control mixtures were added to each sample (supplemental Figure S6). The predefined molar concentration ratios of the spike-in RNAs were used to assess sample quality control and fine-tune bioinformatics analyses.

Following a strategy to minimise potential bulk effects, samples were distributed across multiple sequencing pathways (see supplementary figure S10). Specifically, samples containing distinct genotypes and time points were distributed across distinct sequencing lanes so that a potential bulk effect in a sequencing lane would only impact one biological replicate.

The sequencing procedures utilised a paired-end stranded protocol. During the preprocessing (read alignment and gene expression level quantification) of the sequencing data, paired-end distance and read strandness were utilised to enhance the accuracy of the bioinformatics infrastructure.

Table S1 in the supplementary material provides the number of readings for each sample.

Bacteria cultures. We utilised three strains of *M. tuberculosis*: the wild-type H37RV, a sigE mutant (ST28) in which the sigE gene was rendered inactive, and a complemented strain (ST29) in which the WT sigE gene was reintroduced in an ectopic locus on the chromosome.

The isolates were routinely grown in 7H9 medium supplemented with ADN (5% albumin, 0.2% dextrose, 0.85% sodium chloride), 0.05% Tween 80, and 0.2% glycerol at 37 degrees Celsius.

For each experiment, cells were grown in rolling bottles (225-mL volume capacity) in 30 to 35 mL modified 7H9 broth containing 20 mM MOPS (morpholinepropanesulfonic acid), pH 6.6, and 25 mM Pi (NaH₂PO₄) and

supplemented with 0.05% Tween 80, 0.02% glycerol, and 0.2% glucose to an optical density at 600 nm (OD₆₀₀) of 0.6 to 0.9. The cells were then extracted, rinsed three times with Pi-free broth, and suspended in Pi-free modified Middlebrook 7H9 broth (20 mM MOPS, pH 6.6, 1.46 g sodium chloride, 0.05% Tween 80, 0.02% glycerol, and 0.2% glucose). For all of the experiments, cells were extracted and collected at time zero (in high-phosphate conditions, prior to washings) and after 6, 12, 24, and 48 hours of incubation.

At each time point, 10 mL of each serial dilution was spotted in duplicate on 7H10 plates supplemented with ADN, 0.05% Tween 80, and 0.2% glycerol. After 21 days of 37°C incubation, CFU were recorded.

RNA sample preparation. Total RNA was extracted from 35-mL cultures using the procedure described previously.

To eliminate DNA contamination in the samples, two or three DNase procedures were administered. 5 micrograms of nucleic acid samples were used to confirm the DNA contamination. The quantity of RNA was determined using a spectrophotometer (Nanodrop), and its quality was assessed using a bioanalyzer (Agilent RNA 6000 Nano kit). Only samples with RIN values of 8/9 were utilised in the subsequent phases.

Samples from three separate experiments (a total of 24 samples) were prepared for RNA-seq. *M. tuberculosis* RNAs were spiked with Ambion ERCC spike-in control mixtures from Thermo Fisher Scientific (Waltham, MA) prior to sequencing. The ERCC standards are comprised of two mixtures of spike-in RNAs with defined molar concentration ratios and four subgroups. Each subgroup consists of 23 transcripts whose lengths and GC contents vary and whose concentrations span a 1e6-fold range. According to supplemental Figure S10, the two ERCC spike-in mixtures were distributed across the 24 samples.

RNA sequencing. All samples were subjected to RNA-seq with the Illumina HiSeq sequencer (Illumina, San Diego, CA). Five libraries were sequenced per channel in multiplexing (Fig. S10). Tagged libraries were constructed using the Illumina TruSeq stranded protocol with rRNA depletion, aggregated, and subjected to 2x 100-bp paired-end sequencing.

Process, map, and tally. Reads were preprocessed with the FASTX toolkit 0.0.13.2 (http://hannonlab.cshl.edu/fastx_toolkit); "fastx_clipper" was used to remove adapter sequences, whereas "fastq_quality_trimmer" was used to trim read ends with Phred-scores below 20 and remove reads shorter than 70 bp. Separate files were created for each library's paired reads (i.e., read pairs that passed data preprocessing) and singletons (reads whose mate was discarded by data preprocessing).

Combining the *M. tuberculosis* H37Rv complete genome (GenBank accession number AL123456.3) with the FASTA sequences of the 92 ERCC RNAs produced the reference for read mapping. Separately, paired reads and singletons were mapped to the reference using Bowtie 2 (56) version 2.2.1, which is optimised for mapping unspliced reads of 50 to 100 bp in length with the parameters "--end-to-end" and "--very-sensitive." Using samtools, mapped singletons and paired reads were merged into a single BAM file.

To generate the GTF file of gene coordinates, we obtained the H37Rv annotations from TubercuList (<http://tuberculist.epfl.ch/>), chose the coding sequences (CDS), and merged them with the ERCC RNA annotations. We quantified the gene expression level in two methods in order to assess the data's dependability and eliminate any bias in the bioinformatics analysis.

First, we implemented the "maxcounts" method described by Finotello et al. By calculating gene expression as the maximum coverage along each CDS (or any genomic feature of interest), maxcounts reduces length bias and is robust in situations where the reads are not uniformly distributed along sequences, as occurs due to sequencing errors and ambiguous read mapping.

Analysis of differential expression. To determine the effect of phosphate deprivation on *M. tuberculosis* gene expression, RNA-seq data from samples collected at 6, 12, and 24 h were compared to 0 h in wild-type ("WT_vs_T0") and mutant ("MU_vs_T0") bacteria.

As the analysis of RNA-seq time-series can lead to the selection of a large number of differentially expressed genes (DEGs), which may include false-positives, we analysed RNA-seq data with FunPat, which has been shown to be robust to noise oscillations in time series experimental data. Funpat was used for the step of selection. It implements the bounded-area method, which calculates for each gene the area A of the region circumscribed by the time series expression profile and a baseline, which is set at the corresponding expression level at 0 h. This study specifically analysed two experimental conditions: WT(t = 0) versus WT(t = 0) and MU(t = 0) versus MU(t = 0). A P value was assigned to each gene by assessing the significance of its bounded area relative to a null hypothesis distribution described by a model of the biological-plus-technical

variability and its dependence on the mean gene expression level, which was derived using a negative binomial model with the tag-wise dispersion, whose parameter estimates were obtained using edgeR.

For comparative purposes, differential expression analysis was also conducted with edgeR using generic linear models ("glmFit" and "glmLRT" functions). For both edgeR and FunPat analyses, differentially expressed genes were identified using a 5% significance level based on Benjamini-Hochberg-adjusted P values from multiple tests. Using R (<https://www.R-project.org/>), analyses were conducted.

Clustering of genes and functional annotation. For each gene in the WT (MU) condition, the average gene expression profile was calculated, i.e., at each time point, the average expression level across the three replicates of the WT (MU) condition was calculated. We performed k-means clustering on the average gene expression profiles of only those genes identified as differentially expressed in WT versus T0 (MU versus T0). Calculating the within-cluster-sum-of-squares (WSS) for various values of k and selecting the k for which the WSS curve displayed a distinct elbow, k = 6 was selected. k-means clustering was performed using the kmeans function of the "stats" R package, with a limit of 10,000 iterations and 1,000 restarts. Prior to k-means clustering, average gene expression profiles were scaled and centred so that clusters contain genes with comparable expression profiles rather than expression levels. Data Sets S1 and S6 of the supplementary material contain the outcomes of k-means clustering.

Using DAVID functional annotation clustering (<https://david.ncifcrf.gov/>), the distinct gene clusters were functionally annotated. DAVID takes as input a list of genes and organises them in subsets of genes with similar biological annotation based on multiple co-occurrences of the functional annotation terms found in multiple sources of biological annotation such as Gene Ontology, KEGG Pathways, BioCarta Pathways, Swiss-Prot Keywords, BBID Pathways, SMART Domains, NIH Genetic Association DB, UniProt Sequence Features, COG/KOG Ontology, NCBI OMIM, InterPro Domains, and PIR Super-Family Names. For each functional subset, we report the principal annotation terms, indicating their significance if their false discovery rate (Benjamini-Hochberg correction of functional enrichment test P values) is below 10%. Data Sets S1 and S6 contain the outcomes of the functional annotation analysis. Using R (<https://www.R-project.org/>), analyses were conducted.

Data availability. Sequencing reads and the gene expression count table (both raw and normalised count data) are accessible through the NCBI's Gene Expression Omnibus (GEO) (10) under the accession number GSE211141.

RESULTS AND DISCUSSION

In this section, we first demonstrate and discuss the dynamics of the transcriptional response to low phosphate of a wild-type strain of *M. tuberculosis*, identifying the main genes involved in the development of the stringent response, e.g., sigE-regulated genes, and describing the major alterations in the electron transport chain and the central carbon metabolism pathways. Second, we investigate the stress response to reduced phosphate in the sigE mutant strain, focusing on the alterations that are unique to this strain, such as the oxidative and acidic stress alterations. In order to accomplish this, we compared the wild-type H37Rv strain (WT) and its isogenic sigE-null mutant ST28 (MU), in which SigE is rendered inactive, to one another. Triple cultures of WT and MU grown in a phosphate-rich medium were rinsed and resuspended in a low-phosphate medium. Prior to exposure to low phosphate (time 0) (high phosphate), RNA was extracted and paired-end Illumina RNA-seq was performed. The resultant sequencing data are accessible on NCBI's Gene Expression Omnibus (GEO) (10) under the accession number GSE211141. Bacteria exposed to low-phosphate media remained viable for at least 48 hours (see supplemental Figure S1). We conclude with a validation of the bioinformatics analysis's results' reliability.

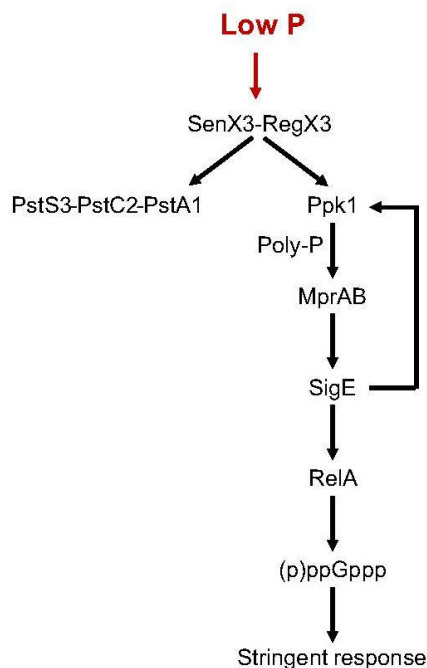


Figure 1: The current stringent response network in *Mycobacterium tuberculosis* is depicted in a schematic. Low phosphate levels activate the two-component system SenX3-RegX3, which in turn induces the phosphate-specific transport operon *pstS3-pstC2-pstA1* and *ppk1*. PPK1 produces PolyP, resulting in a more effective activation of the MprAB two-component system (using PolyP as a substrate for MprB phosphorylation). MprB phosphorylation facilitates sigE activation. SigE enhances the expression of its regulon genes, such as *ppk1* and *relA*.

Analysis of H37Rv wild-type strain

Functional annotation of differentially expressed genes. Differential expression analysis was performed using both edgeR and FunPat (11), considering the entire time course, i.e., at time 6, 12, and 24 h versus time zero, in order to define a gene as differentially expressed (see Materials and Methods for more information).

We identified 2,087 differentially expressed (DE) genes, i.e., genes significantly affected by phosphate deprivation in the *M. tuberculosis* wild-type at 6, 12, and 24 h versus 0 h ("WT versus T0") (see Data Set S1 in the supplementary material).

Gene expression profiles were scaled to their maximum and clustered with k-means into 6 distinct clusters containing 362, 326, 404, 220, 447, and 238 genes (Fig. 2; see also Data Set S1). Using DAVID functional annotation clustering, the various clusters were functionally annotated and characterised by specific patterns for *Mycobacterium tuberculosis* H37Rv. Data Set S1 contains the complete list of WT versus T0 DE genes, the list of genes in each cluster, and the functional terms significantly enriched in each cluster.

Cluster 1 is distinguished by a 12 h peak of upregulation relative to time zero. Lipid catabolism (enoyl-CoA hydratase genes) and protein biosynthesis (aminoacyl-tRNA synthetases) were among the significantly enriched functional terms.

Cluster 2 is characterised by an increasing expression pattern with a 24-hour apex. Significantly enriched functional terms correspond to lipid biosynthesis (i.e. triacylglycerols and 2,3-diacyltrehaloses), response to nitric oxide and hypoxia, as well as PPE family proteins.

Cluster 3 is characterised by a decreasing pattern of expression beginning 6 h after phosphate deprivation and is significantly enriched with functional terms associated with the electron transport chain (menaquinone biosynthesis, NADH dehydrogenases), redox proteins (iron-sulfur cluster assembly), aromatic amino acid, and histidine biosynthesis.

Cluster 4 is characterised by upregulation relative to time zero, with a peak at 6 h, and significant association with functional terms associated with phthiocerol dimycocerosate (PDIM) synthesis.

Cluster 5 exhibits a decreasing expression pattern with downregulation relative to time zero and significantly enriched annotation of the following terms: ribosome synthesis and activity (ribosomal proteins, ribonucleoproteins, RNA-binding proteins, structural constituent, cytosolic large ribosomal subunit), DNA modification enzymes (nucleases, transposases), and toxins (VapC family).

At 12 h, the expression level of Cluster 6 reaches a plateau after a pattern of increasing expression. Cofactors and nucleotide biosynthesis are enriched annotation terms.

Collectively, these clusters confirm that *M. tuberculosis* undergoes a transcriptional metabolic change in response to phosphate deprivation, manifested by a decrease in ribosome biogenesis and RNA transcription. Detailed examples include the repression of *rpoAB* (see Data Set S2 in the supplementary material), encoding the RNA polymerase, indicating a general decrease in transcription, and the expression of a number of genes encoding ribosomal proteins.

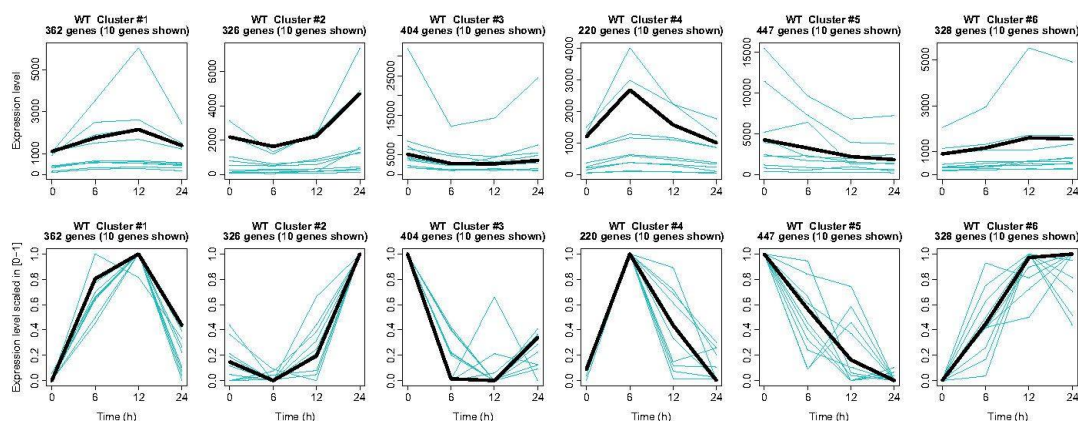


Figure 2: Clustering of genes with differential expression between WT and T0. The figure depicts the six gene clusters generated by k-means clustering. For each cluster, the gene expression profile of the centroid, i.e., the average of all gene expression profiles in the cluster, is displayed in black, along with 10 (randomly selected) gene expression profiles from the same cluster (cyan). Gene expression profiles are depicted on the original scale in the first row to illustrate the variance in gene expression level intensities. In the second panel, the same gene expression profiles are scaled from 0 to 1 to emphasise the profile's shape.

SigE network and SenX3-RegX3 regulon in H37Rv

Exposure to a low-phosphate environment induced several genes known to be directly regulated by SigE (*sigE*, *hsp*, *htpX*, *sigB*, *rv2743- pspA-clgR*, *rv2052c-rv2053c*, and *rv1072-rv1073*) (Data Set S2), as well as genes indirectly regulated by SigE via other regulators that are part of its regulon. These genes encode chaperons, proteases, proteins involved in sulfolipids biosynthesis, and membrane stabilisation and aberrant membrane protein degradation proteins. In a low-phosphate environment, the cell experiences surface stress, likely due to the unfolding of surface proteins, which activates the SigE response, according to these findings.

In accordance with the model of Sanyal et al. increased transcription of the genes encoding the two-component system SenX3-RegX3 was observed in the WT in low-phosphate environments, even though the increase of *senX3* did not attain statistical significance. After 6 h of exposure to minimal phosphate, the expression began to increase and continued to increase until the end of the experiment (Fig. 3A; see also Data Set S2). The same pattern was observed for the phosphate transport operon *pstS3-pstC2-pstA1* (Fig. 3B; Data Set S2), known to be under transcriptional control of the two-components system SenX3-RegX3 (7, 14), but not for the other phosphate transport operons *pstB-pstS1-pstC1-pstA2* (Fig. 3C; Data Set S2) and *pknD-pstS2* (Fig. 3D; Data Set S2). In this instance, the former showed a decrease in expression from the commencement of the experiment, whereas the latter showed a decrease in expression during the first 6 h of exposure to the low-phosphate environment, followed by a recovery after an additional 6 h of exposure. In previous studies, the latter two operons were shown to be either not differentially expressed or only minimally induced in low phosphate, possibly owing to strain and experimental condition differences.

Ppk1, encoding a poly-phosphate kinase, is also known to be regulated by SenX3-RegX3; its SigE-dependent transcription is activated by the binding of phosphorylated RegX3 to its proximal region. Increased *Ppk1* levels

result in an increase in cytoplasmic polyP, a well-known stress signal, which, upon activation of the two-component system MprAB, induces sigE, thereby creating a feed-forward loop between Ppk1 and SigE. Indeed, ppk1 was elicited 12 hours after exposure to low phosphate, when sigE expression peaked (Data Set S2).

Ppk1 was also reported to be essential for the activation of the stringent response via the SigE-dependent induction of relA; in our experiment, relA expression showed an increasing trend beginning 6 h after exposure to a low-phosphate environment, although this increase was not statistically significant (Data Set S2).

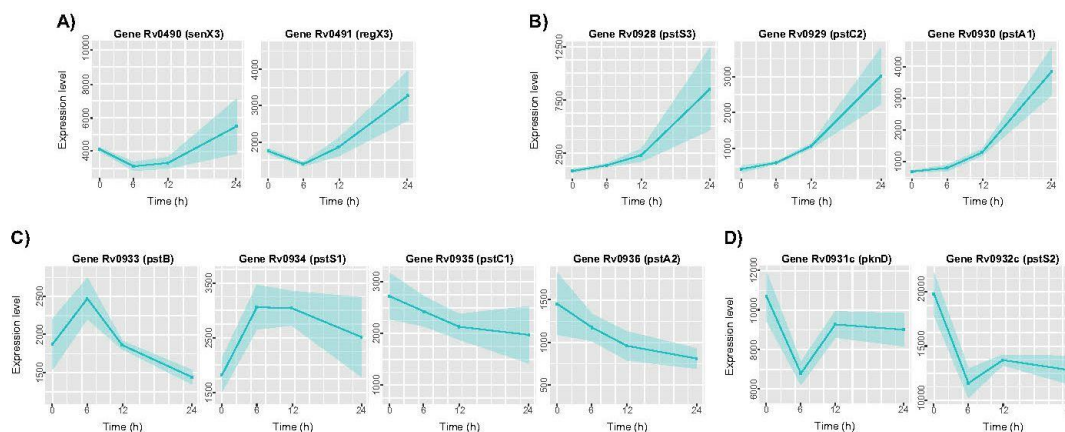


Figure 3: In the wild-type strain, there is differential expression of the gene implicated in phosphate homeostasis. The graphs illustrate the expression profiles of genes encoding proteins directly implicated in the detection of phosphate availability and phosphate assimilation. (A) System with two components. regX3, sensory transduction protein; senX3, sensor histidine kinase. (B) Transport of phosphate operon. pstS3 is a periplasmic phosphate-binding lipoprotein, and pstC2-pstA1 is an ABC-type phosphate transporter. (C) Transport of phosphate operon. pstB is a phosphate-transport ATP-binding protein; pstS1 is a periplasmic phosphate-binding lipoprotein; and pstC1-pstA2 are integral membrane phosphate-transport ABC transporters. pknD, transmembrane serine/threonine-protein kinase; pstS2, periplasmic phosphate-binding lipoprotein.

Changes in electron-transport chain

Reduced supply of cells with Pi for ATP-synthase is an obvious consequence of phosphate deficiency, resulting in decreased ATP production. ATP synthase cannot reimport protons released in the periplasmic space by NADH dehydrogenase type I and cytochrome bc-aa when this enzyme's activity is attenuated. This accumulation of protons in the periplasmic space causes acidification and a change in the proton motive force (pmf). Consistent with this hypothesis, phosphate limitation induces transcription of the membrane carbonic anhydrase CanA (rv1284) gene in *M. tuberculosis* (see Data Sets S3 and S4 in the supplemental material). In addition, several respiratory chain genes are differentially expressed (Fig. 4; Data Sets S3 and S4), which may contribute to the protection of cells from acidification and altered pmf.

(i) The proton-translocating NADH dehydrogenase typeI (nuoABCDEFGHJKLMN) operon (nuoABCDEFGHJKLMN) is downregulated, reducing the export of protons into the periplasmic space. NADH reoxidation can be facilitated by two non-proton-translocating NADH dehydrogenases (type II) Ndh and NdhA, whose expression does not vary.

(ii) The genes involved in the menaquinone biosynthetic pathway (entC-menD-menE) are downregulated, indicating that the density of electron flux across the respiratory chain decreases, thereby diminishing the protons exported from the cell.

(iii) The cytochrome bd oxidase genes (cydCDBA), which encode a non-proton-translocating terminal oxidase with high oxygen affinity, are strongly induced, thereby contributing to further decrease the burden of exported protons and ensuring the continuity of electron flux.

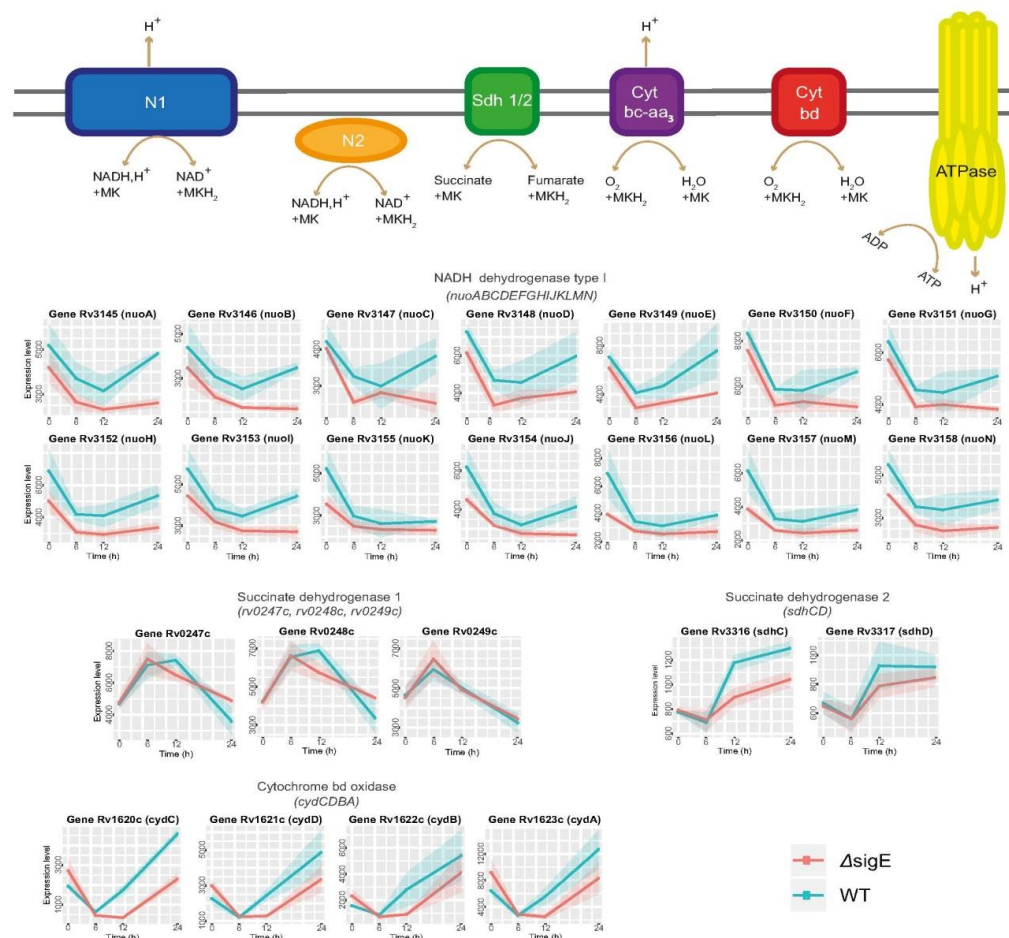


Figure 4: Genes of the electron transport chain are differentially expressed. Enzyme complexes of the respiratory chain are represented schematically at the top. The graphs with cyan/pink lines depict the expression level profiles of involved genes in both the wild-type (WT) (cyan) and the sigE-null mutant (Δ sigE) (pink). Cyt bc-aa₃, cytochrome bc-aa₃ oxidase. Cyt bd, cytochrome bd oxidase.

Central carbon metabolism pathways alteration

The expression of genes encoding enzymes involved in the Krebs cycle is an additional transcriptional response to low phosphate that is intriguing. Isocitrate lyases (*icl1*, *aceAa*, *aceAb*) and succinyl-CoA synthetase (*sucCD*) were induced (Fig. 5; see Data Set S5 in the supplemental material). When there is a substantial decrease in ATP levels and an increase in PMF, such as in hypoxia or iron deficiency, it is known that the pathways involved in succinate production are overexpressed and a small amount of succinate may be secreted to maintain PMF. Our data strongly support a decrease in electron transport chain (ETC) activity, which likely contributes to a decrease in ATP production and a change in pmf. *M. tuberculosis* may increase its production of succinate in low-phosphate environments in order to maintain the pulmonary microflora. (Figure 5; Data Set S5). Comparing this expression pattern to those of isocitrate dehydrogenase 2 (*icd2*) and *sucCD* (Fig. 5), which exhibit only transient induction, suggests that the cell may accumulate α -ketoglutarate. This metabolite is a key metabolic modulator, and a recent study in *Bacteroides thetaiotaomicron* revealed that during stringent response, α -ketoglutarate pool size increases, modifying metabolic processes and promoting growth arrest. When phosphate levels are low in *M. tuberculosis*, it is possible that the accumulated α -ketoglutarate is partially converted to succinate and partially utilised as a metabolic regulator. Expression of succinate dehydrogenase 1 complex (*Sdh1/rv0247c-rv0249c*) decreased between 6 and 12 hours, while expression of succinate dehydrogenase 2 (*Sdh2/sdhCDAB*) increased (Fig. 5; Data Set S5). This change is consistent with the previously demonstrated role of *Sdh2* in stressful conditions, causing a decrease in ATP production, as in hypoxia.

Finally, it was discovered that the genes encoding phosphoenolpyruvate carboxykinase PckA, malate dehydrogenase Mdh, and fumarase Fum were induced (Figure 5; Data Set S5). In a condition in which the high-ATP yielding pathway is impaired, the induction of pckA may represent a substrate-level phosphorylation mechanism to supply ATP, resulting in the production of oxaloacetate. Under these conditions, Fum and Mdh can use the phosphoenolpyruvate-derived oxaloacetate to initiate a reverse Krebs cycle leading to succinate production and NADH reoxidation (Figure 5). In *M. tuberculosis* exposed to hypoxia, a reversal of the oxaloacetate-malate-succinate branch of the Krebs cycle and a glyoxylate shunt have been shown to increase succinate production.

To confirm these hypotheses, targeted metabolomics investigations will be necessary. Recent transcriptomic, proteomic, and metabolomic investigations on *M. tuberculosis* exposed to bedaquiline (BDQ), an inhibitor of membrane-embedded Fo domain of ATPase and therefore mimicking the reduced phosphate effect, partially confirm our hypothesis. In response to BDQ exposure, (i) glyoxylate shunt and anaplerotic PckA are both active, (ii) succinate is secreted, and (iii) in addition to succinate, malate and fumarate are also secreted, raising the possibility that malate and fumarate produced by a reductive Krebs cycle branch in low phosphate can be secreted to maintain an energised membrane. In addition, non-proton-translocating cytochrome bd oxidase (cydAB) is elevated in response to exposure to BDQ and low phosphate.

In support of our hypothesis regarding the acidification of periplasmic space, a transcriptomic study demonstrates that *M. tuberculosis* exposed to mildly low pH downregulates NADH dehydrogenase I and upregulates cytochrome bd oxidase, similarly to what we observed after exposure to low phosphate.

In conclusion, our transcriptomic data indicate that *M. tuberculosis* experiences acidic and high pmf stress during growth in a low-phosphate environment, and to counteract these perturbations, it (i) upregulates carbonic anhydrase expression as a proton sink, and (ii) upregulates phosphomannose dehydrogenase expression as a proton source (iii) secretes tricarboxylic acids to maintain an energised membrane, and (iv) uses sub-stratum-level phosphorylation to maintain ATP production.

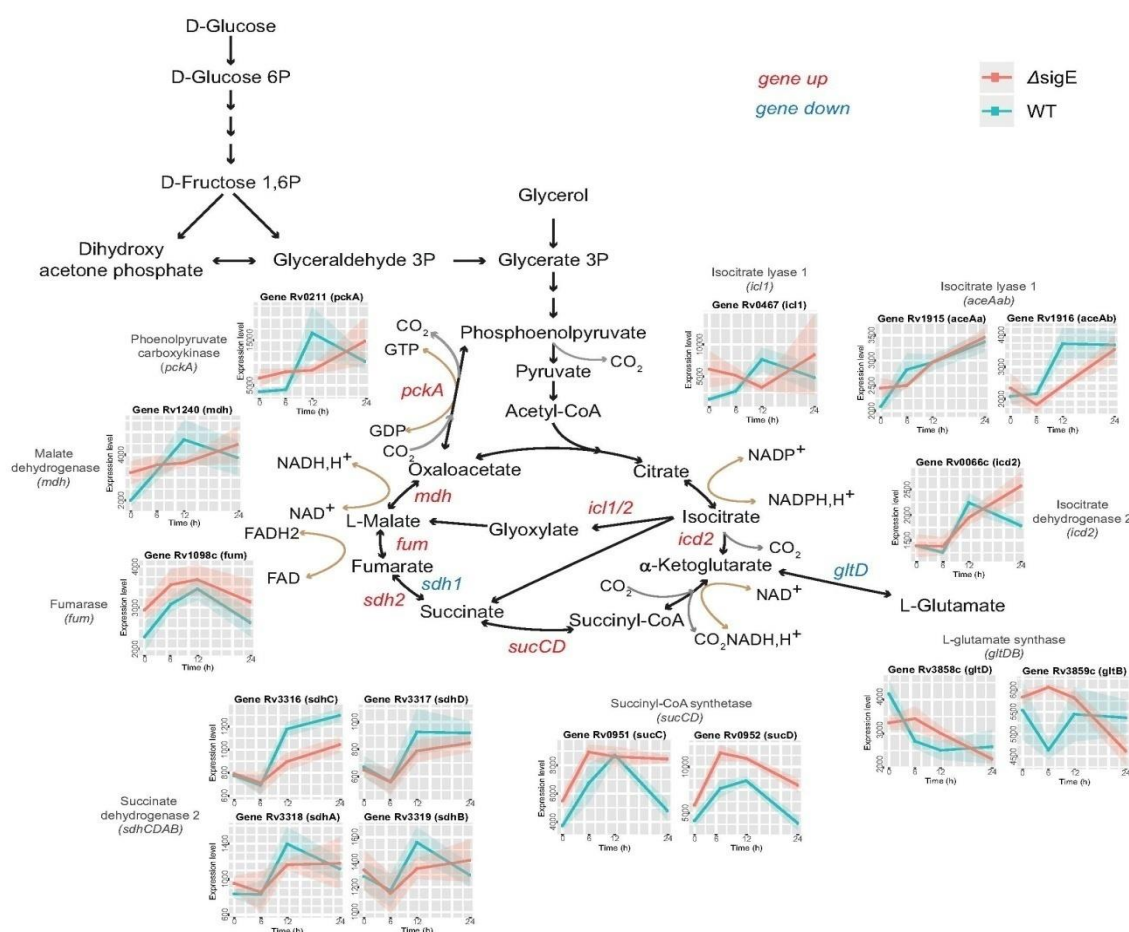


Figure 5: Differential gene expression in the central carbon metabolism. The cyan/pink line graphs depict the expression level profiles of involved genes in both the wild-type (WT) (cyan) and the sigE-null mutant (DsigE)

(pink). Those genes that are up-expressed at 6, 12, and 24 h relative to time zero are highlighted in red, whereas those that are down-expressed are highlighted in blue.

Analysis of the *sigE*-null mutant strain

Functional annotation of differentially expressed genes. When we performed the same analyses on the mutant strain, we discovered that 1,734 genes were significantly affected by phosphate deprivation at 6, 12, and 24 h relative to 0 h (henceforth "MU versus T0"). (refer to Data Set S6 in the supplementary material).

The expression profiles of 310, 311, 406, 279, 185, and 243 genes were clustered using k-means to identify clusters of genes with similar expression profiles (Figure 6). We found that a number of clusters exhibited the same temporal patterns as clusters found in the WT. Some of them were significantly enriched with functional terms with similar meaning. The complete list of MU versus T0 DE genes, the list of genes in each cluster, and the functional terms significantly enriched in each cluster are available in Data Set S6.

Cluster 1 was characterised by temporal profiles comparable to those observed in the same cluster in WT, with significant associations to functional terms associated with DNA binding and transcriptional regulation, including several genes encoding toxin/antitoxin systems and histone-like proteins.

In addition, clusters 2, 3, 4, and 5 exhibited similar temporal profiles to those of the corresponding WT clusters and shared the same functional terms that were enriched.

Cluster 6 exhibited a decreasing expression pattern relative to time 0 at 6 and 12 h, an increasing expression pattern between 12 and 24 h, and significant enrichment terms similar to cluster 2 of the WT.

Interestingly, several typical biological processes associated with the stringent response, such as the downregulation of transcription of ribosomal proteins and RNA polymerase, were also present in the *sigE* mutant, indicating that the fundamental stringent response does not rely on this sigma factor. This was further substantiated by the fact that, despite being expressed at a lower level in the mutant strain, *relA* was induced similarly in both the wild-type and mutant strains.

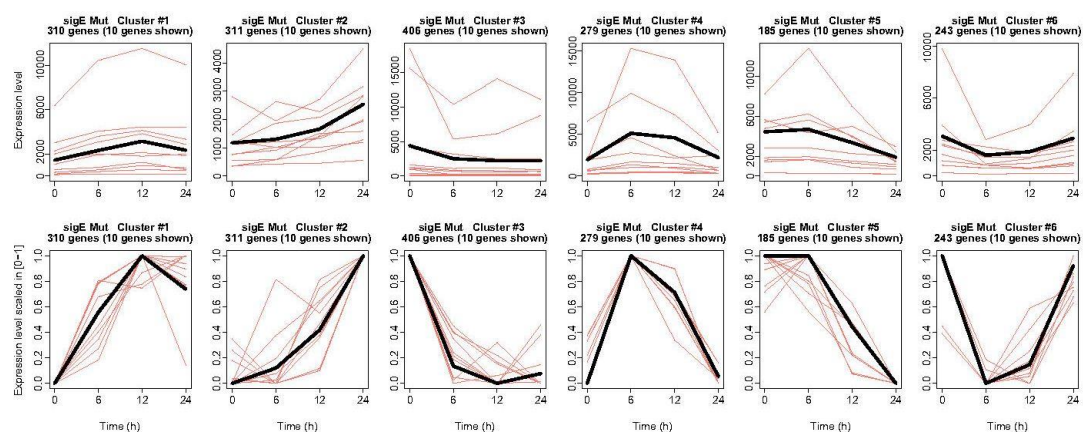


Figure 6: Clustering of genes with differential expression between MU and T0. The k-means algorithm generated six clusters of genomes. For each cluster, the gene expression profile of the centroid, i.e., the average of all gene expression profiles in the cluster, is displayed in black, along with 10 (randomly selected) gene expression profiles from the same cluster (salmon/pink). Gene expression profiles are depicted on the original scale in the first row to illustrate the variance in gene expression level intensities. In the second panel, the same gene expression profiles are scaled from 0 to 1 to emphasise the profile's shape.

SigE network and SenX3-RegX3 regulon in *sigE* mutant

As expected, the genes induced in WT under the control of SigE, SigB, and ClgR were not induced in MU, and in some instances, they displayed a very low level of expression even at time zero (*sigB*, *clgR*; Fig. 7; see also Data Set S7 in the supplementary material). The only exception was the highly expressed and induced *sigE* gene. In our *sigE*-null mutant, the *sigE* gene was disrupted by a Hyg cassette and not completely deleted;

therefore, the first portion of the gene was still expressed. Using DNA microarrays, the overexpression of this portion of the gene in the mutant was previously identified.

In the *sigE* mutant strain, the transcriptional profiles of the genes encoding the two-component system SenX3-RegX3 and the phosphate-transport systems were similar to those observed in the WT strain, with the exception of the operon *pknD-pstS2*, in which the peak of expression at 12 h was absent, indicating a regulatory role for SigE (Data Set S7). As predicted, the induction of *ppk1* was completely abrogated in the mutant, confirming its dependence on SigE (Data Set S7). However, *relA* followed a similar temporal pattern in the two strains, but its level of expression was significantly lower in the mutant (Figure 7), suggesting that even if SigE plays a role in phosphate-starvation conditions, other sigma factors can, at least partially, compensate for its absence. A candidate is SigH, whose consensus sequence is extremely similar to that of SigE, and which was induced in the *sigE* mutant strain but not in the wild-type strain (Fig. 7; Data Set S7). Since RelA is primarily regulated at the posttranslational level, it is unclear whether the reduced expression of *relA* in the *sigE* mutant affects the activation of the stringent response. In a *sigE* mutant complementation strain, wild-type levels of *sigB* expression and *ppk1* induction were restored (see Figs. S2 and S3 in the supplementary material).

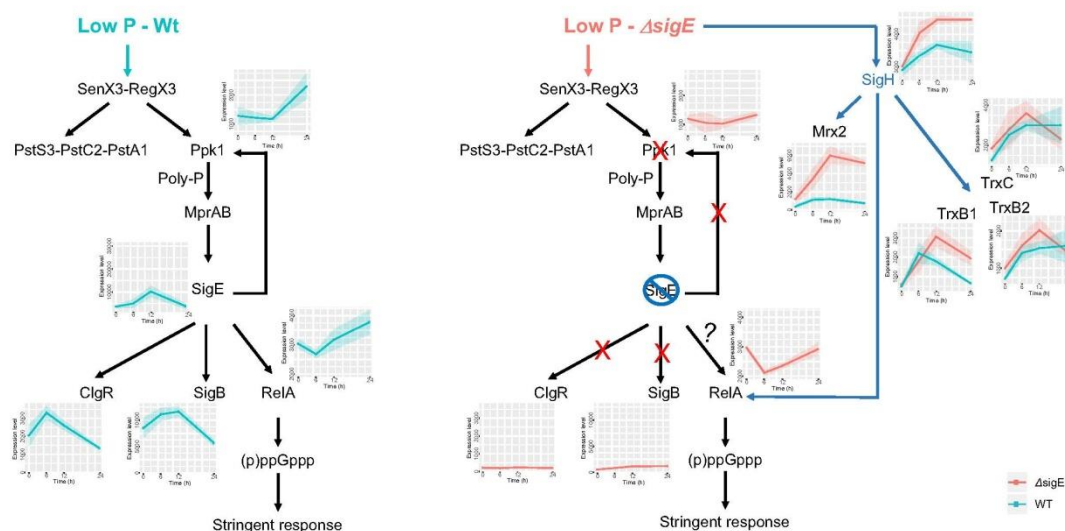


Figure 7: Schematic depiction of the stringent response network in *M. tuberculosis* WT and *sigE* mutant strains demonstrating the induction of SigE-dependent genes in response to low pH, which is completely abolished in the *sigE*-null mutant, as well as the induction of *sigH* and related genes in the *sigE* mutant. The cyan/pink line graphs depict the expression level profiles of involved genes in both the wild-type (WT) (cyan) and the *sigE*-null mutant (*ΔsigE*) (pink).

Oxidative and acid stress in *sigE* mutant

One of the most remarkable differences between the transcriptional profiles of the two strains was the induction of *sigH* and its regulon in the *sigE* mutant (see Data Sets S3 and S8 in the supplemental material), which is known to be essential for protection from oxidative stress.

Genes of the SigH regulon found to be upregulated in the *sigE* mutant (Fig. 7) in response to low phosphate included those encoding the protein disaggregase ClpB (rv0384c), an important regulator of the stress response; three genes encoding the TRX system designed to protect cells from oxidative damage (*trxB*-rv1471, *trxB2*-rv3913, *trxC*-rv3914); and rv2466c-*mrx2*, encoding a mycoredoxin (Fig. 7; Data Set S8). Notably, genes involved in mycothiol biology, such as rv0486-*mshA* and rv1082-*mca*, were induced in this mutant, despite not being known to be regulated directly by SigH (Data Set S8). In a *sigE* mutant complementation strain, the induction of *sigH* and *mrx2* was abolished (see Fig. S4 in the supplementary material). While SigH and mycothiol have always been linked to the oxidative stress response, several studies have also linked them to the response to low pH, suggesting that *sigE* exposed to low phosphate may experience either one or both of these stress conditions. It is unclear why the absence of SigE may result in acidic and/or oxidative stress; therefore, additional experiments are required to shed light on this topic. The primary function of SigE is to

protect the cell envelope against surface stress. It is possible that the alterations in the electron transport chain induced in low phosphate to reduce electron flux and control pH cause the membrane to lose homeostasis, thereby activating the SigE response, which is capable of maintaining membrane integrity. In its absence, however, the envelope could be damaged, interfering with the correct functionality of the electron transport chain and the acid-protection system, resulting in the production of reactive oxygen species (ROS) and the modification of the photovoltaic field (pmf).

Strong induction in the sigE mutant of the genes encoding the lipoprotein Rv1540 and the phospholipase Rv2037c (Data Set S8), which are both involved in the maintenance of the cell envelope integrity under stress, but are not part of the SigE regulon, confirms that this mutant experiences cell envelope stress under phosphate limitation.

Other alterations specific to the sigE mutant

In support of our hypothesis that the sigE mutant undergoes a significant change in electron transport chain activity, we observed induction of the gene encoding the well-known transcriptional factor WhiB6, which responds to changes in redox potential.

In addition, we discovered other genes specifically induced in the sigE mutant, which may indicate that this strain is subjected to a greater degree of stress than WT, although it is unclear how these changes are functionally linked to the absence of SigE. Specifically, we discovered the following to be induced: (i) whiB7, which encodes a transcriptional regulator (Data Set S9) that modulates the expression of several genes involved in intrinsic resistance to translation-targeting antibiotics, such as eis, rv1258, and the op-eron rv0492c-rv0493c; (ii) genes encoding multidrug-efflux pumps, such as mmpL5-mmpS5, rv26.

Robustness and reproducibility of the RNA-seq results

To evaluate the reproducibility of this study's key findings, we analysed the dependability of RNA-seq data and the robustness of the bioinformatics pipeline.

More than 99.8 percent of the RNA-seq reads passed the quality control test and were considered for alignment (see Table S1 in the supplementary materials). The read alignment step yielded a high proportion of mapped reads ranging from 97.41% to 99.66%; read alignment statistics are provided in Table S1. The read mapping statistics confirmed the absence of contaminants, the high efficiency of rRNA depletion, and the fabrication of stranded libraries (see Tables S1 and S2 in the supplementary material).

The robustness of the bioinformatics infrastructure was evaluated by comparing various strategies for gene expression level quantification and differential gene expression analysis.

Regarding the quantification of gene expression levels, we utilised two alternative approaches, namely "totcounts" and "maxcounts" (see Materials and Methods). Regardless of the adopted gene expression level quantification strategy, there is a high degree of concordance between biological replicates, as evidenced by a Pearson correlation of >0.95 and >0.95 for maxcounts and totcounts, respectively (see Figs. S5 to S8 in the supplementary material). These results indicate the absence of batch effects in the data and the independence of the computed gene expression levels from the quantification strategy. Remarkably, the adoption of a stranded protocol and a high sequencing depth enhanced the precision of estimated gene expression levels. In light of the substantial agreement between the two quantification strategies and the demonstrated robustness of the maxcounts strategy to read length bias and irregular coverage, gene expression levels were quantified using maxcounts in this study.

The other essential phase in the bioinformatics analysis is the identification of differentially expressed genes (DEGs), as the analysis of the RNA-seq time-series can lead to the selection of a large number of DEGs that are likely to contain false-positives. Both edgeR, one of the most extensively used tools for RNA-seq data analysis, and FunPat, a tool developed specifically for the analysis of time series RNA-seq data, were utilised for differential expression analysis. FunPat selected a smaller number of DEGs than edgeR (see Fig. S9A in the supplementary material). Notably, between 93.84 and 97.65 percent of all DEGs chosen by FunPat were also chosen by edgeR. In addition, we evaluated the false positives (FP) generated by FunPat and edgeR by examining external RNA controls consortium (ERCC) spike-in RNAs (n = 23) with constant concentration in all RNA-seq libraries that were identified as differentially expressed by the two methods. FunPat demonstrated

greater control over the FP-rate than edgeR (see Table S3 in the supplementary material). Due to the high concordance between DEGs identified by both methods and the superior control of the FP rate provided by FunPat, DEGs identified by FunPat were utilised in this study. FunPat was also evaluated on totcounts data to further evaluate the robustness of differential expression analysis. The list of DEGs derived with the two methodologies revealed a substantial overlap (Fig. S9B), but a marginally greater number of FPs were identified from totcounts data than maxcounts data (Table S3).

Overall, the aforementioned tests validated the dependability of the generated RNA-seq data, the robustness of the adopted bioinformatics infrastructure, and the reproducibility of the bioinformatics analysis' principal finding.

Conclusions

Our data support the hypothesis that SigE is not directly involved in the activation of the stringent response, despite the fact that its induction along with its regulon genes was clearly confirmed at low phosphate levels. Nonetheless, our data suggest that under these conditions, its function is to counteract the stress that the drastic alteration of cellular metabolism imposes on the cells. In the absence of SigE, another sigma factor, SigH, along with other transcriptional regulators, such as WhiB6 and WhiB7, serve as a failsafe system to assist the cell in adapting to the new physiologic conditions.

REFERENCES

1. Baek SH, Li AH, Sasseti CM. 2011. Metabolic regulation of mycobacterial growth and antibiotic sensitivity. *PLoS Biol* 9:e1001065.
2. Baker JJ, Johnson BK, Abramovitch RB. 2014. Slow growth of *Mycobacterium tuberculosis* at acidic pH is regulated by phoPR and host-associated carbon sources. *Mol Microbiol* 94:56–69.
3. Barik S, Sureka K, Mukherjee P, Basu J, Kundu M. 2010. RseA, the SigE specific anti-sigma factor of *Mycobacterium tuberculosis*, is inactivated by phosphorylation-dependent ClpC1P2 proteolysis. *Mol Microbiol* 75: 592–606.
4. Baruzzo G, Hayer KE, Kim EJ, Di Camillo B, FitzGerald GA, Grant GR. 2016. Simulation-based comprehensive benchmarking of RNA-seq aligners. *Nat Methods* 14:135–139.
5. Basu P, Sandhu N, Bhatt A, Singh A, Balhana R, Gobe I, Crowhurst NA, Mendum TA, Gao L, Ward JL, Beale MH, McFadden J, Beste DJV. 2018. The anaplerotic node is essential for the intracellular survival of *Mycobacterium tuberculosis*. *J Biol Chem* 293:5695–5704.
6. Boldrin F, Provvedi R, Cioetto Mazzabò L, Segafreddo G, Manganelli R. 2020. Tolerance and persistence to drugs: a main challenge in the fight against *Mycobacterium tuberculosis*. *Front Microbiol* 11:1924.
7. Borisov VB, Gennis RB, Hemp J, Verkhovsky MI. 2011. The cytochrome bd respiratory oxygen reductases. *Biochim Biophys Acta* 1807:1398–1413.
8. Buchmeier N, Fahey RC. 2006. The mshA gene encoding the glycosyl-transferase of mycothiol biosynthesis is essential in *Mycobacterium tuberculosis* Erdman. *FEMS Microbiol Lett* 264:74–79.
9. Casonato S, Provvedi R, Dainese E, Palù G, Manganelli R. 2014. *Mycobacterium tuberculosis* requires the ECF sigma factor SigE to arrest phagosome maturation. *PLoS One* 9:e108893.
10. Chen Z, Hu Y, Cumming BM, Lu P, Feng L, Deng J, Steyn AJC, Chen S. 2016. Mycobacterial WhiB6 differentially regulates ESX-1 and the Dos regulon to modulate granuloma formation and virulence in zebrafish. *Cell Rep* 16:2512–2524.
11. Cook GM, Greening C, Hards K, Berney M. 2014. Energetics of pathogenic bacteria and opportunities for drug development. *Adv Microb Physiol* 65: 1–62.
12. Coulson GB, Johnson BK, Zheng H, Colvin CJ, Fillingner RJ, Haiderer ER, Hammer ND, Abramovitch RB. 2017. Targeting *Mycobacterium tuberculosis* sensitivity to thiol stress at acidic pH kills the bacterium and potentiates antibiotics. *Cell Chem Biol* 24:993–1004.
13. Covarrubias AS, Larsson AM, Högbom M, Lindberg J, Bergfors T, Björkelid C, Mowbray SL, Unge T, Jones TA. 2005. Structure and function of carbonic anhydrases from *Mycobacterium tuberculosis*. *J Biol Chem* 280:18782–18789.

14. Danchik C, Wang S, Karakousis PC. 2021. Targeting the Mycobacterium tuberculosis stringent response as a strategy for shortening tuberculosis treatment. *Front Microbiol* 12:2970.
15. Das, Priyanka & Janahiraman, V (2019). Analytical Study on Heterocyclic Anticancer Compounds. *Research Review International Journal of Multidisciplinary*; 4(5):172-175.
16. Das, Priyanka & Janahiraman, V (2019). Study on New Chalcones and Nitrogen Containing Heterocyclics. *International Journal of Scientific Research And Review*; 8(5):1069-1080.
17. Das, Priyanka & Srivastav, Alok Kumar (2014). Phytochemical Extraction and Characterization of the Leaves of *Andrographis paniculata* for Its Anti-Bacterial, Anti-Oxidant, Anti-Pyretic and Anti-Diabetic Activity. *International Journal of Innovative Research in Science Engineering and Technology*; 3(8):15176-15184.
18. Das, Priyanka & Srivastav, Alok Kumar (2015). A Comparative Study on Nutritive Values of Several Vegetables from West Bengal, Eastern India. *International Journal of Pharmaceutical Research and Bio-Science*; 4(1):381-390.
19. Das, Priyanka & Srivastav, Alok Kumar (2015). In-vitro Micropropagation of The Miracle Plant Aloe vera - A Method of Rapid Production. *International Journal of Pure and Applied Research in Engineering and Technology*; 3(11):12-27.
20. Das, Priyanka & Srivastav, Alok Kumar (2015). Phytochemical Extraction And Characterization of the Leaves of *Aloe vera barbadensis* For Its Anti-Bacterial And Anti-Oxidant Activity. *International Journal of Science and Research*; 4(6):658-661.
21. Das, Priyanka & Srivastav, Alok Kumar (2015). To Study the Effect of Activated Charcoal, Ascorbic Acid and Light Duration on In-vitro Micropropagation of Aloe vera L. *International Journal of Innovative Research in Science Engineering and Technology*; 4(5):3131-3138.
22. Das, Priyanka & Srivastav, Alok Kumar (2021). A Study on Molecular Targeted Approaches To Cancer Therapy And The Role of Chalcones In Chemoprevention. *European Journal of Molecular & Clinical Medicine*; 8(3):3254-3267.
23. de Souza GA, Leversen NA, Målen H, Wiker HG. 2011. Bacterial proteins with cleaved or uncleaved signal peptides of the general secretory pathway. *J Proteomics* 75:502–510.
24. Di Camillo B, Toffolo G, Nair SK, Greenlund LJ, Cobelli C. 2007. Significance analysis of microarray transcript levels in time series experiments. *BMC Bioinformatics* 8:S10.
25. Edgar R, Domrachev M, Lash AE. 2002. Gene Expression Omnibus: NCBI gene expression and hybridization array data repository. *Nucleic Acids Res* 30:207–210.
26. Eoh H, Rhee KY. 2013. Multifunctional essentiality of succinate metabolism in adaptation to hypoxia in *Mycobacterium tuberculosis*. *Proc Natl Acad Sci U S A* 110:6554–6559.
27. Finotello F, Lavezzo E, Bianco L, Barzon L, Mazzon P, Fontana P, Toppo S, Di Camillo B. 2014. Reducing bias in RNA sequencing data: a novel approach to compute counts. *BMC Bioinformatics* 15:S7.
28. Fontán PA, Aris V, Alvarez ME, Ghanny S, Cheng J, Soteropoulos P, Trevani A, Pine R, Smith I. 2008. *Mycobacterium tuberculosis* sigma factor E regulon modulates the host inflammatory response. *J Infect Dis* 198:877–885.
29. Ghodke, Babasaheb Shivanath, Das, Priyanka & Srivastav, Alok Kumar (2022). An Analytical Study to Understand the Mechanism Behind Derailing the Aspartate Pathway of *Mycobacterium Tuberculosis* to Eradicate Persistent Infection. *International Journal For Innovative Research In Multidisciplinary Field*; 8(7):78-90.
30. Ghodke, Babasaheb Shivanath, Yadav, Sakshi (2021). Disrupting *Mycobacterium Tuberculosis* Aspartate Pathway in Order To Eliminate a Chronic Infection. *Webology*; 18(2):2571-2588.
31. Ghodke, Babasaheb Shivanath, Yadav, Sakshi (2022). An Insight Into The Exploration At The Molecular Level About The Role Of Stringent Response In *Mycobacterium Tuberculosis* Dormancy. *Journal of Pharmaceutical Negative Results*; 13(1):2486-2498.
32. Glover RT, Kriakov J, Garforth SJ, Baughn AD, Jacobs WR. 2007. The two-component regulatory system *senX3-regX3* regulates phosphate-dependent gene expression in *Mycobacterium smegmatis*. *J Bacteriol* 189:5495–5503.
33. Hartman T, Weinrick B, Vilchèze C, Berney M, Tufariello J, Cook GM, Jacobs WR. 2014. Succinate dehydrogenase is the regulator of respiration in *Mycobacterium tuberculosis*. *PLoS Pathog* 10:e1004510.
34. Haurlyuk V, Atkinson GC, Murakami KS, Tenson T, Gerdes K. 2015. Recent functional insights into the role of (p)ppGpp in bacterial physiology. *Nat Rev Microbiol* 13:298–309.

35. Huang DW, Sherman BT, Lempicki RA. 2009. Systematic and integrative analysis of large gene lists using DAVID bioinformatics resources. *Nat Protoc* 4:44–57.
36. Huergo LF, Dixon R. 2015. The emergence of 2-oxoglutarate as a master regulator metabolite. *Microbiol Mol Biol Rev* 79:419–435.
37. Irving SE, Choudhury NR, Corrigan RM. 2021. The stringent response and physiological roles of (pp)pGpp in bacteria. *Nat Rev Microbiol* 19:256–271.
38. Koul A, Vranckx L, Dhar N, Göhlmann HWH, Özdemir E, Neefs JM, Schulz M, Lu P, Mørth E, McKinney JD, Andries K, Bald D. 2014. Delayed bactericidal response of *Mycobacterium tuberculosis* to bedaquiline involves remodelling of bacterial metabolism. *Nat Commun* 5:3369.
39. Kumari B, Saini V, Kaur J, Kaur J. 2020. Rv2037c, a stress induced conserved hypothetical protein of *Mycobacterium tuberculosis*, is a phospholipase: role in cell wall modulation and intracellular survival. *Int J Biol Macromol* 153:817–835.
40. Langmead B, Salzberg SL. 2012. Fast gapped-read alignment with Bowtie 2. *Nat Methods* 9:357–359.
41. Lew JM, Kapopoulou A, Jones LM, Cole ST. 2011. TubercuList–10 years after. *Tuberculosis (Edinb)* 91:1–7.
42. Li H, Handsaker B, Wysoker A, Fennell T, Ruan J, Homer N, Marth G, Abecasis G, Durbin R, 1000 Genome Project Data Processing Subgroup. 2009. The sequence alignment/map format and SAMtools. *Bioinformatics* 25:2078–2079.
43. Lu J, Holmgren A. 2014. The thioredoxin antioxidant system. *Free Radic Biol Med* 66:75–87.
44. M. 2007. Polyphosphate kinase is involved in stress-induced mprAB-sigE-related signalling in mycobacteria. *Mol Microbiol* 65:261–276.
45. Mackenzie JS, Lamprecht DA, Asmal R, Adamson JH, Borah K, Beste DJV, Lee BS, Pethe K, Rousseau S, Krieger I, Sacchetti JC, Glasgow JN, Steyn AJC. 2020. Bedaquiline reprograms central metabolism to reveal glycolytic vulnerability in *Mycobacterium tuberculosis*. *Nat Commun* 11:6092.
46. Målen H, Pathak S, Sjøfteland T, de Souza GA, Wiker HG. 2010. Definition of novel cell envelope associated proteins in Triton X-114 extracts of *Mycobacterium tuberculosis* H37Rv. *BMC Microbiol* 10:132.
47. Manganelli R, Voskuil MI, Schoolnik GK, Dubnau E, Gomez M, Smith I. 2002. Role of the extracytoplasmic-function sigma factor sigma(H) in *Mycobacterium tuberculosis* global gene expression. *Mol Microbiol* 45:365–374.
48. Manganelli R, Voskuil MI, Schoolnik GK, Smith I. 2001. The *Mycobacterium tuberculosis* ECF sigma factor sigma E: role in global gene expression and survival in macrophages. *Mol Microbiol* 41:423–437.
49. Manganelli R. 2007. Polyphosphate and stress response in mycobacteria. *Mol Microbiol* 65:258–260.
50. McCarthy DJ, Chen Y, Smyth GK. 2012. Differential expression analysis of multifactor RNA-Seq experiments with respect to biological variation. *Nucleic Acids Res* 40:4288–4297.
51. Milano A, Pasca MR, Provvedi R, Lucarelli AP, Manina G, Luisa de Jesus Lopes Ribeiro A, Manganelli R, Riccardi G. 2009. Azole resistance in *Mycobacterium tuberculosis* is mediated by the MmpS5-MmpL5 efflux system. *Tuberculosis (Edinb)* 89:84–90.
52. Pathak R, Rathor N, Garima K, Sharma NK, Singh P, Varma-Basil M, Bose M. 2015. IspA gene of *Mycobacterium tuberculosis* co-transcribes with Rv1540 and induced by surface and acidic stress. *Gene* 560:57–62.
53. Preiss L, Langer JD, Yildiz Ö, Eckhardt-Strelau L, Guillemont JEG, Koul A, Meier T. 2015. Structure of the mycobacterial ATP synthase Fo rotor ring in complex with the anti-TB drug bedaquiline. *Sci Adv* 1:e1500106.
54. Prusa J, Zhu DX, Stallings CL. 2018. The stringent response and *Mycobacterium tuberculosis* pathogenesis. *Pathog Dis* 76:fty054.
55. Ramón-García S, Ng C, Jensen PR, Dosanjh M, Burian J, Morris RP, Folcher M, Eltis LD, Grzesiek S, Nguyen L, Thompson CJ. 2013. WhiB7, an Fe-S-dependent transcription factor that activates species-specific repertoires of drug resistance determinants in actinobacteria. *J Biol Chem* 288:34514–34528.
56. Rawat M, Uppal M, Newton G, Steffek M, Fahey RC, Av-Gay Y. 2004. Targeted mutagenesis of the *Mycobacterium smegmatis* mca gene, encoding a mycothiol-dependent detoxification protein. *J Bacteriol* 186:6050–6058.
57. Rifat D, Bishai WR, Karakousis PC. 2009. Phosphate depletion: a novel trigger for *Mycobacterium tuberculosis* persistence. *J Infect Dis* 200:1126–1135.

58. Robinson MD, McCarthy DJ, Smyth GK. 2010. edgeR: a Bioconductor package for differential expression analysis of digital gene expression data. *Bioinformatics* 26:139–140.
59. Rosado LA, Wahni K, Degiacomi G, Pedre B, Young D, De la Rubia AG, Boldrin F, Martens E, Marcos-Pascual L, Sancho-Vaello E, Albesa-Jové D, Provvedi R, Martin C, Makarov V, Versées W, Verniest G, Guerin ME, Mateos LM, Manganelli R, Messens J. 2017. The antibacterial prodrug activator Rv2466c is a mycothiol-dependent reductase in the oxidative stress response of *Mycobacterium tuberculosis*. *J Biol Chem* 292:13097–13110.
60. Sanavia T, Finotello F, Di Camillo B. 2015. FunPat: function-based pattern analysis on RNA-seq time series data. *BMC Genomics* 16:S2.
61. Sanyal S, Banerjee SK, Banerjee R, Mukhopadhyay J, Kundu M. 2013. Polyphosphate kinase 1, a central node in the stress response network of *Mycobacterium tuberculosis*, connects the two-component systems MprAB and SenX3-RegX3 and the extracytoplasmic function sigma factor, sigma E. *Microbiology (Reading)* 159:2074–2086.
62. Schofield WB, Zimmermann-Kogadeeva M, Zimmermann M, Barry NA, Goodman AL. 2018. The stringent response determines the ability of a commensal bacterium to survive starvation and to persist in the gut. *Cell Host Microbe* 24:120–132.
63. Serafini A, Boldrin F, Palù G, Manganelli R. 2009. Characterization of a *Mycobacterium tuberculosis* ESX-3 conditional mutant: essentiality and rescue by iron and zinc. *J Bacteriol* 191:6340–6344.
64. Serafini A. 2021. Interplay between central carbon metabolism and metal homeostasis in mycobacteria and other human pathogens. *Microbiology (Reading)* 167:e001060.
65. Song T, Song SE, Raman S, Anaya M, Husson RN. 2008. Critical role of a single position in the -35 element for promoter recognition by *Mycobacterium tuberculosis* SigE and SigH. *J Bacteriol* 190:2227–2230.
66. Srivastav, Alok Kumar & Das, Priyanka (2014). Phytochemical Extraction and Characterization of Roots of *Withania somnifera* for Its Anti-Bacterial, Anti-Oxidant, Anti-Inflammation and Analgesic Activity. *International Journal of Innovative Research and Development*; 3(7):22-33.
67. Srivastav, Alok Kumar & Das, Priyanka (2014). To Study the Formulation of Niosome of Ofloxacin and Its Evaluation for Efficacy of Anti-Microbial Activity. *International Journal of Innovative Research in Science Engineering and Technology*; 3(12):17958-17965.
68. Srivastav, Alok Kumar & Das, Priyanka (2015). A Comparative Study of the Effect of Ampicillin and Tetracyclin on Bacterial Culture by Measuring the Zone of Inhibition. *International Journal of Pharmaceutical Research and Bio-Science*; 4(1):277-285.
69. Srivastav, Alok Kumar & Das, Priyanka (2015). Phytochemical Extraction and Characterization of *Acorus calamus*, *Moringa oliefera*, *Cucurbita maxima*, *Hibiscus rosa sinensis* and *Chrysanthemum leucanthemum* For Their Anti-Bacterial and Anti-Oxidant Activity. *International Journal of Pharmaceutical Research and Bio-Science*; 4(3):356-377.
70. Srivastav, Alok Kumar & Das, Priyanka (2015). To Study the Production and Standardization of Veterinary Vaccines. *International Journal of Science and Research*; 4(6):2331-2337.
71. Srivastav, Alok Kumar & Janahiraman, V (2019). Microbial Synthesis of Hyaluronan and Its Biomedical Applications. *International Journal of Scientific Research And Review*; 8(5):852-863.
72. Srivastav, Alok Kumar & Janahiraman, V (2019). Study on Microbial Production of Hyaluronic Acid. *Research Review International Journal of Multidisciplinary*; 4(5):231-233.
73. Srivastav, Alok Kumar & Suriyakala, P.C. (2022). Hyaluronic Acid Generated by *Streptococcus zooepidemicus* is Recovered Utilising PEG-Citrate Aqueous Two Phase Systems. *Journal of Pharmaceutical Negative Results*; 13(1):100-108.
74. Srivastav, Alok Kumar & Suriyakala, P.C. (2023). Biotechnological Production and Purification of Hyaluronic Acid from *Streptococcus zooepidemicus*. *Journal of Pharmaceutical Negative Results*; 14(2):78-83.
75. Sureka K, Dey S, Datta P, Singh AK, Dasgupta A, Rodrigue S, Basu J, Kundu
76. Tripathi P, Parijat P, Patel VK, Batra JK. 2018. The amino-terminal domain of *Mycobacterium tuberculosis* ClpB protein plays a crucial role in its substrate disaggregation activity. *FEBS Open Bio* 8:1669–1690.
77. Vanzembergh F, Peirs P, Lefevre P, Celio N, Mathys V, Content J, Kalai M. 2010. Effect of PstS sub-units or PknD deficiency on the survival of *Mycobacterium tuberculosis*. *Tuberculosis (Edinb)* 90:338–345.

78. Vilchèze C, Av-Gay Y, Attarian R, Liu Z, Hazbón MH, Colangeli R, Chen B, Liu W, Alland D, Sacchetti JC, Jacobs WR. 2008. Mycothiol biosynthesis is essential for ethionamide susceptibility in *Mycobacterium tuberculosis*. *Mol Microbiol* 69:1316–1329.
79. Vilchèze C, Weinrick B, Leung LW, Jacobs WR. 2018. Plasticity of *Mycobacterium tuberculosis* NADH dehydrogenases and their role in virulence. *Proc Natl Acad Sci U S A* 115:1599–1604.
80. Watanabe S, Zimmermann M, Goodwin MB, Sauer U, Barry CE, Boshoff HI. 2011. Fumarate reductase activity maintains an energized membrane in anaerobic *Mycobacterium tuberculosis*. *PLoS Pathog* 7:e1002287.
81. World Health Organization. 2021. Global tuberculosis report 2021. World Health Organization, Geneva, Switzerland. <https://www.who.int/publications/i/item/9789240037021>. Retrieved 11 February 2022.